Grain boundary complexions: The interplay of premelting, prewetting, and multilayer adsorption

Jian Luo[a)]
School of Materials Science and Engineering, Clemson University, Clemson, South Carolina 29634, USA

(Received 9 July 2009; accepted 3 August 2009; published online 21 August 2009)

A thermodynamic model for coupled adsorption and disordering transitions at grain boundaries is developed by combining diffuse-interface and lattice-gas models and incorporating colloidal type interfacial forces. This model produces a systematical spectrum of interfacial phenomena for grain boundaries, including first-order and continuous coupled prewetting and premelting transitions, critical points, multilayer adsorption, layering and roughening, and complete wetting and drying, and it produces a series of grain boundary "phases" (complexions) with character similar to those observed by [Dillon *et al.*, Acta Mater. **55**, 6208 (2007)]. The presence of dispersion and electrostatic forces in ceramic materials can appreciably change grain boundary transitions. © *2009 American Institute of Physics*. [DOI: 10.1063/1.3212733]

Grain boundaries (GBs) can exhibit "phase" transitions, which will drastically change transport, mechanical, and physical properties.[1,2] One example is GB premelting in unary systems.[3] In multicomponent systems, GB disordering can be enhanced by concurrent adsorption. Consistently, stabilization of subsolidus quasiliquid intergranular films (IGFs) has been reported for Ni-doped W,[4] Ni-doped Mo,[5] and other multicomponent materials.[1,2] Using a generalized Cahn critical point wetting (diffuse-interface) model, Tang *et al.*[6] suggested that subsolidus IGFs form from coupled GB prewetting and premelting transitions. Most recently, another diffuse-interface (phase-field) model[7] and atomistic simulation[8] of GB premelting in Ag-doped Cu have been reported.

On the other hand, impurity-based IGFs have been widely observed in structural and functional ceramics,[1] where such IGFs can control sintering, creep resistance, and electronic properties.[1] The presence of vdW London dispersion (vdW-Ld) and electrical double-layer (EDL) forces in ceramic systems complicates GB phenomena.[1] In 2007, Dillon *et al.*[9] observed six distinct GB complexions (phases) in doped Al_2O_3; each complexion exhibits characteristic width, structural disorder, and mobility. This discovery helped to reveal the origin of abnormal grain growth.[9]

A long-range scientific goal is to develop quantitative GB "phase" or complexion diagrams as a tool for the mechanism-informed materials design.[9,10] To support this goal, this letter reports a generic thermodynamic model that produces the most systematical spectrum of GB transitions and critical phenomena to date. This model (1) treats through-thickness compositional and structural gradients, (2) considers the finite atomic size effects, and (3) enables the convenient incorporation of vdW-Ld, EDL and other interfacial forces.

Following Tang *et al.*,[6] the present model considers three field variables: composition (X), crystallinity (η), and orientation (θ). As illustrated in Fig. 1, this model assumes that the atomic layers inside the grains are discrete, where each layer has a constant thickness (δ) but different X_i and η_i; on the other hand, the liquidlike GB core (i.e., an IGF) exhibits spatially varying $X(x)$ and $\eta(x)$ profiles, as well as a continuous thickness (h). The abrupt crystal-film interfaces are automatically resulted from the energy minimization, which has been explained using a diffuse-interface theory[11] and is supported by high-resolution transmission electron microscopy observations.[1]

At a fixed temperature (T) and bulk composition (X_B), the equilibrium GB structure is obtained by minimizing the excess free energy (using a constrained minimization function in MATLAB):

$$\gamma_{GB}(T,X_B)=\min_{(\eta_i,X_i,h_0)}\left\{2\delta\sum_{i=2}^{\infty}\left[\Delta f_V(X_i,\eta_i)+\frac{\kappa_X}{\delta^2}\cdot(X_i-X_{i-1})^2+\frac{\kappa_\eta}{\delta^2}\cdot(\eta_i-\eta_{i-1})^2\right]+\sigma_{CORE}(X_1,\eta_1,h_0)+\sigma_{INT}(h)\right\} \quad (1)$$

with respect to a set of adjustable parameters (X_i, η_i, and h_0). The boundary conditions are $X_\infty=X_B$ and $\eta_\infty=1$. In Eq. (1) [and Eq. (2)], Δf_V is the excess volumetric free energy with respect to a reference state set by the crystalline grains (X_B and $\eta=1$). Gradient coefficients k_X and k_η are estimated from regular solution parameters (Ω) and fusion enthalpy (ΔH_{fuse})

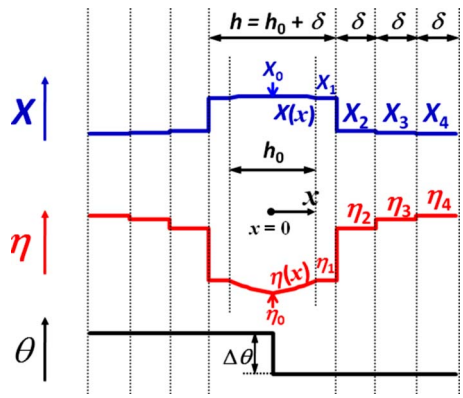

FIG. 1. (Color online) Schematic illustration of a GB structure.

a)Electronic mail: jluo@alum.mit.edu.

based on lattice-gas[12] and Miedema-type[13] interfacial energy models. The first term (the sum) in Eq. (1) can be considered as a lattice-gas model[12] that is extended to include an additional field variable of crystallinity. The excess free energy of the GB core is formulated following Tang *et al.*:[6]

$$\sigma_{\mathrm{CORE}}(X_1,\eta_1,h_0) \equiv \delta\cdot\Delta f_V(X_1,\eta_1)+\min_{\eta(x),X(x)}\left(2\int_0^{h_0/2}\left\{\Delta f_V[X(x),\eta(x)]+\kappa_X\cdot\left(\frac{dX}{dx}\right)^2+\kappa_\eta\cdot\left(\frac{d\eta}{dx}\right)^2\right\}dx+s|\Delta\theta|\cdot\eta_0^2\right), \quad (2)$$

where $X(x)$ and $\eta(x)$ should be adjusted to minimize the functional with the boundary conditions of $X(h_0/2)=X_1$ and $\eta(h_0/2)=\eta_1$. Then, $\eta_0[=\eta(0)]$ and $X_0[=X(0)]$ can be solved for a given set of h_0, η_1, and X_1. Tang *et al.*[6] showed that $\theta(x)$ adopts a step function (Fig. 1); in Eq. (2), $s|\Delta\theta|\cdot\eta_0^2$ is an energy penalty related to the misorientation between the two grains ($\Delta\theta$), where s is a coefficient.[6] A normalized misorientation is defined as

$$\Theta\equiv(0.5s\delta/\kappa_\eta)\cdot|\Delta\theta|\equiv\gamma_{\mathrm{GB}}^{(0)}/(2\gamma_{\mathrm{CL}}^{(0)}), \quad (3)$$

where $\gamma_{\mathrm{GB}}^{(0)}$ and $\gamma_{\mathrm{CL}}^{(0)}$ are excess free energies of a "perfectly dry" GB and a "perfectly sharp" crystal-liquid interface, respectively (which are different from the equilibrium γ_{GB} and γ_{CL}). The $X(x)$ and $\eta(x)$ profiles that minimize $\sigma_{\mathrm{CORE}}(X_1,\eta_1,h_0)$ can be obtained by numerically solving the corresponding Euler equations. For quicker computations, a useful analytical approximation for the minimized energy $\sigma_{\mathrm{CORE}}(X_1,\eta_1,h_0)$ can be readily derived after expanding Δf_V into a Taylor series and omitting high order terms.

This model is carefully formulated to avoid unphysical behaviors due to a discrete layer thickness effect in the submonolayer adsorption region. In Fig. 1 and Eq. (2), $h(=h_0+\delta; h_0\geq 0)$ adopts a value between δ and $+\infty$ that minimizes the excess free energy and a liquidlike IGF exhibits through-thickness gradients only if $h>\delta$. After h_0 reaches zero, the GB excess can be further reduced by reducing X_1 (thus the "equivalent thickness" of adsorbates can be reduced below one monolayer).

Additional interfacial interactions [the third term in Eq. (1)] can be expressed as

$$\sigma_{\mathrm{INT}}(h)=\sigma_{\mathrm{OS}}(h) \quad [+\sigma_{\mathrm{vdW}}(h)+\sigma_{\mathrm{EDL}}(h)+\ldots]. \quad (4)$$

The first term is an oscillatory structural interaction that arises from a finite atom size effect.[10,14] Since statistical mechanics showed that the oscillatory periodicity and characteristic decay length for the analogous solvation forces in colloidal systems are both close to the molecular size,[15] the following phenomenological term is adopted:

$$\sigma_{\mathrm{OS}}(h)\approx-\Delta\gamma_{\mathrm{OS}}\cdot\cos(2\pi h/\delta)\cdot e^{-h/\delta}, \quad (5)$$

where $\Delta\gamma_{\mathrm{OS}}$ is introduced to scale the magnitude of this interaction, and the energy minima are presumed to occur at $h\approx n\delta$ where n is an integer (being slightly different from the case of solvation forces with two hard walls). An accurate expression of $\sigma_{\mathrm{OS}}(h)$ should be derived from classical density functional theories in future studies, and the presence of multiple bond lengths will likely complicate this interaction. For ceramics, vdW-Ld and EDL forces can also be added. These interfacial energy terms, e.g., the vdW-Ld force, also depend on the compositional/structural profile. Incorporating $\sigma_{\mathrm{INT}}(h)$ of typical strengths does not noticeably affect the adsorption and disordering behaviors in the monolayer and submonolayer regimes, but it can appreciably change the multilayer adsorption character (Figs. 3 and 4).

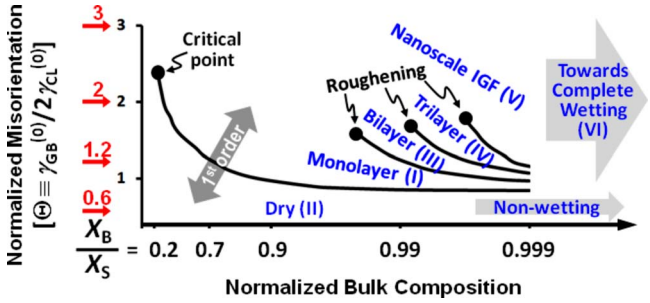

FIG. 2. (Color online) A representative GB diagram computed using the model and parameters given in the text. First-order transition lines and critical points are plotted in the field of normalized bulk composition $[-\log_{10}(1-X_B/X_S)]$ and normalized GB misorientation [Θ as defined in Eq. (3)]. GB phases and the associated Dillon–Harmer complexion numbers (I-VI) are labeled.

Figure 2 is a representative GB "phase" diagram computed for a binary regular solution A-B with the following parameters: temperatures (T=2000 K, $T_{m,A}$=3000 K, and $T_{m,B}$=1500 K), regular solution parameters (Ω_S=60 kJ/mol and Ω_L=3 kJ/mol), molar volume and layer distance ($V=10^{-5}$ m^3/mol and δ=0.255 nm), fusion entropies (10 J/mol K), the energy barrier parameter (5.63 kJ/mol), and solidus and liquidus compositions (X_S=0.0109 and X_L=0.4797). $\Delta f_V(X,\eta)$ is constructed using a standard interpolation method in phase-field modeling (see, e.g., Ref. 6). For the results shown in Figs. 2 and 3, $\Delta\gamma_{\mathrm{OS}}$ is set to be 0.5 mJ/m^2 [$\Delta\gamma_{\mathrm{OS}}$=0 as a reference for the dashed lines in Fig. 3(a)], and vdW-Ld and EDL forces are not included.

Important features in the GB diagram shown in Fig. 2 include a first-order coupled prewetting and premelting transition line, which terminates at a GB critical point (above which the transition becomes continuous), and multiple first-order layering transition lines, which terminates at respective GB roughening (critical) points. Figure 3 shows the computed GB excess, η_0 and X_0 versus bulk composition (X_B) for GBs of different normalized misorientations (Θ=0.6–3.0). Four representative curves computed for Θ=0.6, 1.2, 2, and 3, respectively, are highlighted. For Θ=0.6, the GB is "dry" ($X_0\ll X_L$ and $\eta>0.5$) for the entire region. For Θ=1.2, a first-order prewetting/premelting transition occurs with increasing X_B, following by a series of first-order layering transitions. These layering transitions, which produces a series of discrete Dillon–Harmer complexions (Fig. 2), stemmed from the oscillatory structural interaction; as a comparison, the dashed lines in Fig. 3(a) are computed assuming $\Delta\gamma_{\mathrm{OS}}$=0, where the GB excess increases continuously in the multilayer adsorption region (noting that the presence of the oscillatory structural force does not appreciably change the primary prewetting/premelting transition line and critical point in the monolayer adsorption region). When Θ is raised to 2, the first-order prewetting/premelting transition persists, but the GB excess increases continuously in the multilayer adsorption region (i.e., above roughening points). Above the primary GB critical point (at $\Theta\approx$2.4 and $X_B\approx 0.225X_S$), the prewetting/premelting transition becomes continuous in the entire region, which is represented by the

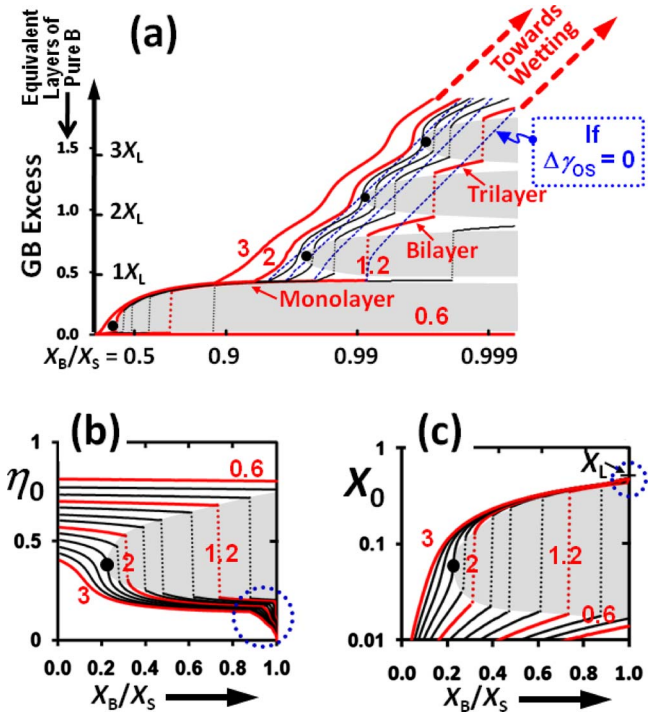

FIG. 3. (Color online) Computed (a) GB excess, (b) $\eta_0[=\eta(0)]$, and (c) $X_0[=X(0)]$ vs bulk composition (X_B). X_S and X_L are the bulk solidus and liquidus compositions, respectively. Different curves represent GBs of different normalized misorientations [$\Theta=0.6-3.0$, with an increment of 0.2 between the adjacent lines; lines computed for $\Theta=2.2-2.8$ are removed in (a) for figure clarity]. Lines computed for selected Θ values of 0.6, 1.2, 2, and 3 are highlighted and labeled, and the corresponding positions in the computed GB diagram are indicated by the arrows in Fig. 2. The solid lines are computed assuming $\Delta\gamma_{OS}=0.5$ mJ/m^2; the dashed lines in (a) are computed assuming $\Delta\gamma_O=0$ (shown only for $\Theta=1.0-1.8$ for figure clarity). First-order transitions tie lines (dotted lines) and critical points (solid circles) are indicated. [(a)–(c)] can be regarded as three alternative representations of the GB diagram shown in Fig. 2, in which the gray colored areas are the GB phase separation regions.

curve computed for $\Theta=3$. The first-order transitions and the primary critical point are also clearly evident in computed η_0 and X_0 curves [Figs. 3(b) and 3(c)]. Small abrupt jumps in computed η_0 and X_0 curves related to the layering transitions (in the multilayer adsorption region) also appear in the circled regions in Figs. 3(b) and 3(c), although the enlarged views are not shown due to the space limit. Figures 3(a)–3(c) can be regarded as three alternative representations of the GB diagram shown in Fig. 2, in which the GB phase separation areas (gray), first-order transitions tie lines (dotted), and critical points (solid circles) are labeled.

Figure 4 shows the computed film thickness (h) versus bulk composition (for $\Theta=1.2$) with and without consideration of the vdW and EDL forces. Plausible values of Hamaker constant ($A_{121}=20$ zJ), surface potential ($\phi_S=300$ mV), and Debye length ($\kappa^{-1}=\delta$) are used to compute Fig. 4(b). Comparison of Figs. 4(a) and 4(b) illustrates that the presence of vdW and EDL forces of typical strengths in ceramic materials can (1) expand the stability regions for complexions III-VI, (2) promote roughening, and (3) inhibit the (otherwise anticipated) complete wetting at the coexistence.

In summary, the interfacial thermodynamic model reported in this letter produces first-order and continuous prewetting/premelting transitions, critical points, multilayer

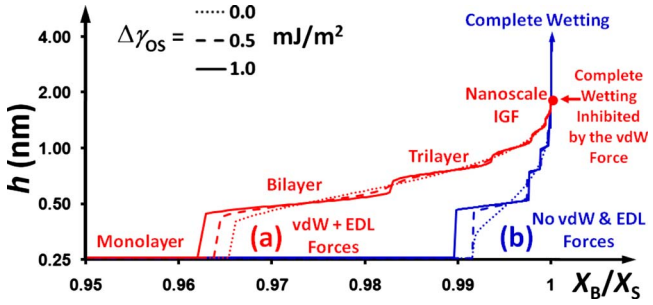

FIG. 4. (Color online) Film thickness (h) vs bulk composition computed (a) with and (b) without the incorporation of vdW-Ld and EDL forces (assuming $\Theta=1.2$). See text and the legend for the specific parameters used for computing this figure.

adsorption, layering and roughening, and complete wetting and drying at binary GBs; this systematic array of interfacial phenomena are analogous to a case of multilayer gas adsorption on attractive inert surfaces.[16] The existence of GB prewetting/premelting transitions was indicated by GB composition and diffusivity measurements for Cu–Bi and Fe–Si–Zn.[2] Similar high-temperature surface complexions have been systematically characterized,[17] where an analogous first-order transition has been directly observed.[18] The occurrence of layering transitions explains the recent observation of six distinct GB complexions by Dillon *et al.*[9] The fact that nanoscale IGFs are more frequently observed in ceramics than metals can be explained from the effects of vdW and EDL forces. This model represents an effort to establish a thermodynamic foundation for developing "GB diagrams" as a tool for mechanism-informed materials design.

This work is sponsored by the U.S. DOE Office of Basic Energy Science (Grant No. DE-FG02-08ER46511 in the DMSE Electron and Scanning Probe Microscopies program, managed by Dr. Jane G. Zhu).

[1] J. Luo, Crit. Rev. Solid State Mater. Sci. **32**, 67 (2007).
[2] B. B. Straumal and B. Baretzky, Interface Sci. **12**, 147 (2004).
[3] A. M. Alsayed, M. F. Islam, J. Zhang, P. J. Collings, and A. G. Yodh, Science **309**, 1207 (2005); J. J. Hoyt, D. Olmsted, S. Jindal, M. Asta, and A. Karma, Phys. Rev. E **79**, 020601 (2009); J. Mellenthin, A. Karma, and M. Plapp, Phys. Rev. B **78**, 184110 (2008); J. Berry, K. R. Elder, and M. Grant, *ibid.* **77**, 224114 (2008).
[4] J. Luo, V. K. Gupta, D. H. Yoon, and H. M. Meyer, Appl. Phys. Lett. **87**, 231902 (2005); V. K. Gupta, D. H. Yoon, H. M. Meyer III, and J. Luo, Acta Mater. **55**, 3131 (2007).
[5] X. Shi and J. Luo, Appl. Phys. Lett. **94**, 251908 (2009).
[6] M. Tang, W. C. Carter, and R. M. Cannon, Phys. Rev. Lett. **97**, 075502 (2006).
[7] Y. Mishin, W. J. Boettinger, J. A. Warren, and G. B. McFadden, Acta Mater. **57**, 3771 (2009).
[8] P. L. Williams and Y. Mishin, Acta Mater. **57**, 3786 (2009).
[9] S. J. Dillon, M. Tang, W. C. Carter, and M. P. Harmer, Acta Mater. **55**, 6208 (2007).
[10] J. Luo, Curr. Opin. Solid State Mater. Sci. **12**, 81 (2008).
[11] J. Luo, M. Tang, R. M. Cannon, W. C. Carter, and Y.-M. Chiang, Mater. Sci. Eng., A **422**, 19 (2006).
[12] I. Shimizu and Y. Takei, Acta Mater. **53**, 811 (2005).
[13] R. Benedictus, A. Böttger, and E. J. Mittemijer, Phys. Rev. B **54**, 9109 (1996).
[14] J. Luo and X. M. Shi, Appl. Phys. Lett. **92**, 101901 (2008).
[15] J. N. Israelachvili, *Intermolecular and Surface Forces*, 4th ed. (Academic, London, 1994).
[16] R. Pandit, M. Schick, and M. Wortis, Phys. Rev. B **26**, 5112 (1982).
[17] J. Luo and Y.-M. Chiang, Annu. Rev. Mater. Res. **38**, 227 (2008).
[18] H. Qian and J. Luo, Acta Mater. **56**, 4702 (2008); H. J. Qian and J. Luo, Appl. Phys. Lett. **91**, 061909 (2007).